

## APPLICATION OF THE HBV HYDROLOGICAL MODEL ON THE ILARION CATCHMENT, GREECE

MARIUS-VICTOR BÎRSAN<sup>1</sup>, BOGDAN POPA<sup>2</sup>, DANIELA POPESCU<sup>1,3</sup>,  
LIANA-IOANA VUȚĂ<sup>2</sup>, ELIZA-ISABELA TICĂ<sup>2</sup>, ION-ANDREI NITA<sup>4</sup>

<sup>1</sup>Institute of Geography, Romanian Academy. Dimitrie Racoviță 12, 023993 Bucharest, Romania.  
E-mail: Marius.Birsan@gmail.com

<sup>2</sup>National University of Science and Technology POLITEHNICA Bucharest, Romania.

<sup>3</sup>National Institute of Hydrology and Water Management. Bucharest Romania.

<sup>4</sup>VisualFlow. Aurel Vlaicu 140, 020099 Bucharest, Romania.

*Received: July 21, 2025*

*Abstract.* The HBV hydrological model simulates the discharge using as input data the daily rainfall and air temperature, and uses conceptual descriptions to represent hydrological processes. Multi-annual means of monthly potential evaporation are used as well. The model describes the water balance using three storage reservoirs – for the soil moisture zone, the upper storage zone (sub-surface flow) and the lower storage zone, respectively. Here we present the application of the model on the Ilarion catchment of the Aliakmon river, which is located in Western Macedonia, northwestern Greece. The river basin has a drainage area of 5014 km<sup>2</sup> and a mean elevation of 917 m.a.s.l., its topography varying from narrow gorges to wide flood plains. The years 1981–2003 were used for calibration and the 2004–2009, for validation. The HBV model managed to reproduce well the observed streamflow while keeping the parameters values physically meaningful.

*Key words:* rainfall-runoff model; Aliakmon River; South-East Europe; Genetic Algorithm and Powell (GAP) optimization; Monte Carlo; conceptual model; performance assessment.

DOI:

### 1. INTRODUCTION

Rainfall-runoff models represent valuable tools for various hydrological applications, like hydrological forecasting, climate change impact studies, spillway design, groundwater response simulations, or water balance mapping [1,2]. This paper deals with the application of the conceptual model HBV (Hydrologiska Byråns Vattenbalansavdelning), which is a general-purpose hydrological model named after the Swedish abbreviation of the Hydrological Bureau Waterbalance department (a former section of the Swedish Meteorological and Hydrological Institute) where the model was originally developed by Sten Bergström and his colleagues. The model

has been applied to hundreds of river basins worldwide – including nival and glacial basins in the Alps, Himalayas, North America, New Zealand and Greenland, arctic basins in Scandinavia and northern Alaska, and basins from humid and semi-arid environments like Tunisia or Panama [3]. The catchment basin areas ranged from few km<sup>2</sup> to over 40 000 km<sup>2</sup>, highlighting the model’s ability to maintain the physical meaning of its parameters across scales.

Here we present the application of the HBV model on a Greek river basin situated in Northern Macedonia region. The model performance was assessed using seven objective metrics for both calibration and validation periods.

## 2. STUDY AREA

The Ilarion catchment is located in northwestern Greece (Fig. 1), on the upper part of the Aliakmon River in Western Macedonia, between latitudes 39°30’–40°30’N and longitudes 20°30’–22°00’E.

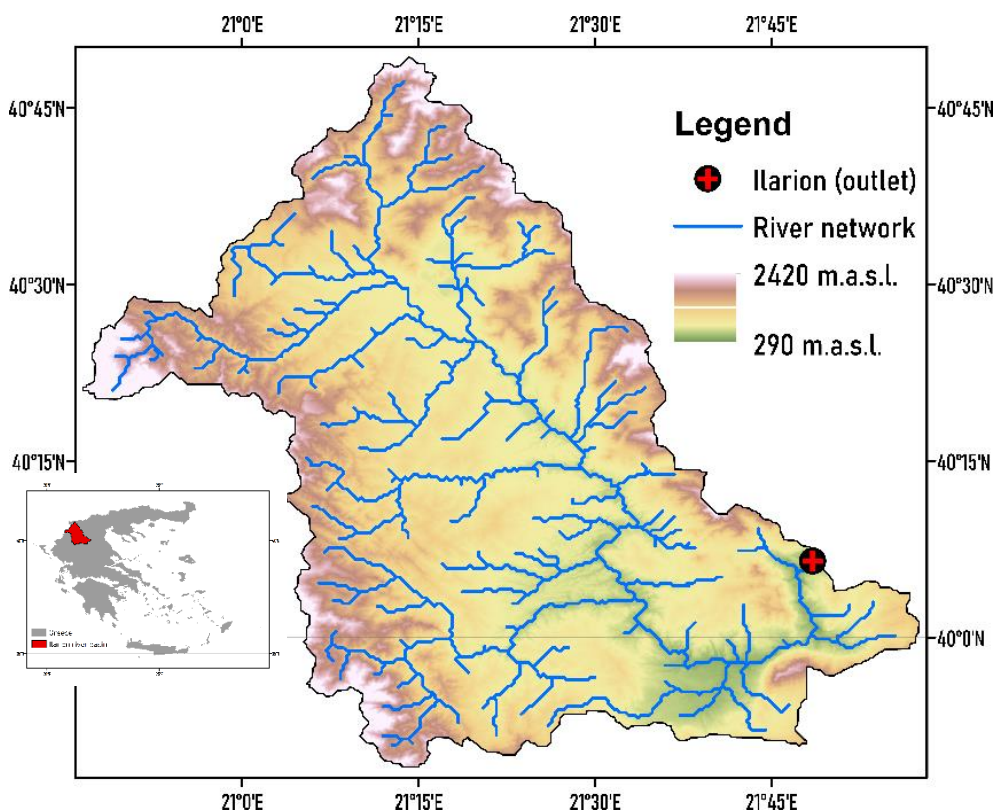


Fig. 1 – Elevation and river network of the Ilarion catchment. The location of the basin in Greece is shown on bottom left.

The river basin has a drainage area of 5014 km<sup>2</sup> and a mean elevation of 917 m.a.s.l. The topography is characterized by narrow gorges and wide vegetated plains without deep slopes. The mean annual temperature is ~11°C and the cumulated precipitation is around ~825 mm per year. The mean annual runoff at the basin outlet is around 49 m<sup>3</sup>/s [4].

### 3. DATA AND METHODS

#### 3.1. DAILY TIME SERIES AND MULTIANNUAL DATA

Daily streamflow data at the outlet of the catchment was obtained from SMHI HypeWeb (<https://hypeweb.se>), an online platform that provides historical hydrological data series. Precipitation and air temperature were extracted from the E-OBS gridded dataset v31.0e, at 0.1°×0.1° spatial resolution for the period 1981-2009 [5]. The years 1981-2003 were used for the calibration of the model, and the last six years (2004-2009) were kept for validation. Multi-annual potential evapotranspiration values over the river basin were extracted from the CHELSA database [6-9] for the period 1981-2010.

#### 3.2. THE HBV HYDROLOGICAL MODEL

HBV is a semi-distributed hydrological model that simulates the discharge using daily rainfall and air temperature as input data [3,10]. HBV uses conceptual descriptions to represent hydrological processes [11]. Multiannual means of monthly potential evaporation are used as well. The model describes the water balance using three storage reservoirs – for the soil moisture zone, the upper storage zone (sub-surface flow) and the lower storage zone, respectively (Fig. 2). Precipitation is simulated to be either snow or rain depending on whether the temperature of the corresponding time step is above or below a threshold,  $TT$  [°C].

All precipitation falling as snow is multiplied by a snowfall correction factor, SFCF. Snowmelt is calculated with the degree-day method (Eq. 1).

$$melt = CFMAX(T(t) - TT) \quad (1)$$

Snowmelt (meltwater) and rainfall are retained within the snowpack until exceeding a certain fraction,  $CWH$ , of the water equivalent of the snow. Liquid water within the snowpack refreezes according to Eq. 2.

$$refreezing = CFR CFMAX(TT - T(t)) \quad (2)$$

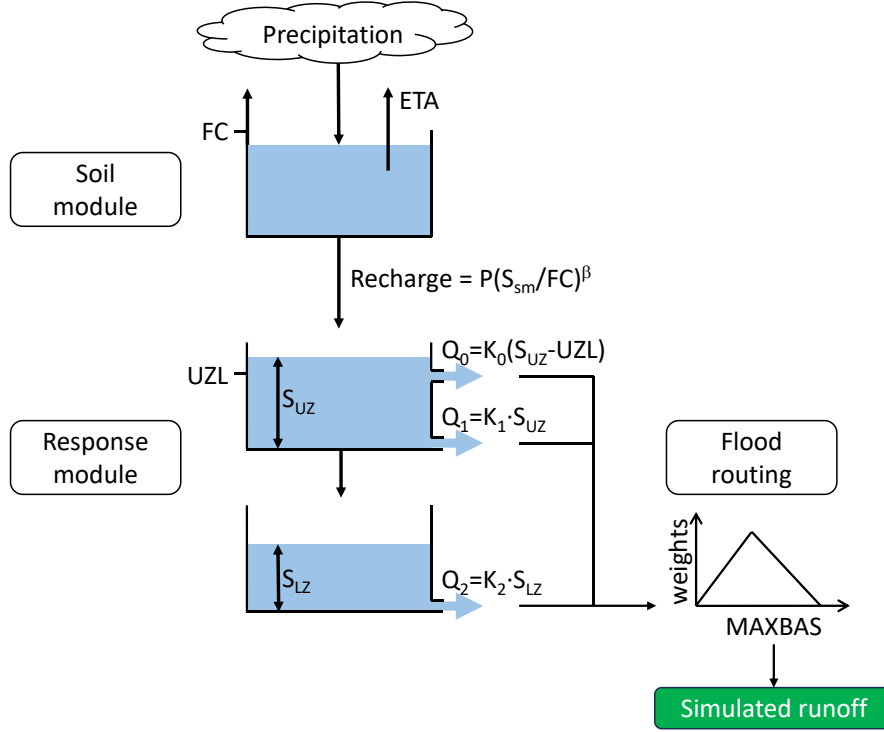


Fig. 2 – Model structure of HBV. Source: Koutsouris et al. (2017), adapted from Seibert (2000).

Rainfall and snowmelt ( $P(t)$ ) are divided into water filling the soil box and groundwater recharge depending on the relation between water content of the soil box ( $SM$  [mm]) and its largest value,  $FC$  [mm] (Eq. 3).

$$\frac{recharge}{P(t)} = \left( \frac{SM(t)}{FC} \right)^{BETA} \quad (3)$$

Actual evaporation from the soil box equals the potential evaporation if  $SM/FC$  is above  $LP$ , while a linear reduction is used when  $SM/FC$  is below  $LP$  (Eq. 4).

$$E_{act} = E_{pot} \cdot \min \left( \frac{SM(t)}{FC \cdot LP}, 1 \right) \quad (4)$$

Groundwater recharge is added to the upper groundwater box,  $SUZ$  [mm].  $PERC$  [mm/day] defines the maximum percolation rate from the upper to the lower groundwater box,  $SLZ$  [mm]. Runoff from the groundwater boxes is computed as the sum of two or three linear outflow equations depending on whether  $SUZ$  is above a threshold value,  $UZL$  [mm], or not (Eq. 5).

$$Q_{GW}(t) = K_2 SLZ + K_1 SUZ + K_0 \cdot \max(SUZ - UZL, 0) \quad (5)$$

This runoff is finally transformed by a triangular weighting function defined by the parameter  $MAXBAS$  (Eq. 6) to give the simulated runoff [mm/day].

$$Q_{sim}(t) = \sum_{i=1}^{MAXBAS} c(i) Q_{GW}(t - i + 1) \quad (6)$$

$$\text{where } c(i) = \int_{i-1}^i \frac{2}{MAXBAS} - \left| u - \frac{MAXBAS}{2} \right| \frac{4}{MAXBAS^2} du$$

If different elevation zones are used the changes precipitation and temperature with elevation are calculated using the two parameters  $PCALT$  [%/100 m] and  $TCALT$  [°C / 100 m] (Eqs. 7,8).

$$P(h) = P_0 \left( 1 + \frac{PCALT(h - h_0)}{10000} \right) \quad (7)$$

$$T(h) = T_0 \left( 1 + \frac{TCALT(h - h_0)}{10000} \right) \quad (8)$$

The long-term mean of the potential evaporation,  $E_{pot,M}$  for a certain day of the year can be corrected to its value at day  $t$ ,  $E_{pot}(t)$ , by using the deviations of the temperature,  $T(t)$ , from its long-term mean,  $T_M$ , and a correction factor,  $CET$  [°C<sup>-1</sup>] (Eq. 9).

$$E_{pot}(t) = (1 + C_{ET}(T(t) - T_M))E_{pot,M} \quad (9)$$

with  $0 \leq E_{pot}(t) \leq 2E_{pot,M}$ .

### 3.3. CALIBRATION APPROACH

Two methods of calibration were used:

(i) *Monte Carlo*. Multiple model runs are made with random parameters. The parameter values are chosen randomly within a given range and the model is run using these parameters. The number of model runs (i.e., generated parameter sets) with the Monte Carlo method was set to 2 million.

(ii) *Genetic Algorithm and Powell optimization (GAP)*. The GAP algorithm optimizes a model parameter set constrained by predefined minimum and maximum values by means of an evolutionary mechanism. The approach tries to further optimize the parameter set using Powell's quadratically convergent method [12] as recommended by Seibert and Vis [13]. The GAP optimization was run independently 500 000 times, with 1000 parameter sets for each population.

The parameter ranges for all variables involved in the calibration process are shown in Table 1. They were adapted from Karamouz et al. [14] and Seibert [12].

*Table 1*  
Minimum and maximum parameter values used for calibration

Module	Parameter	Description	Units	Min	Max
<b>Snow accumulation and melting</b>	<i>TT</i>	Temperature threshold for snow/rain	°C	-2.5	2.5
	<i>CFMAX</i>	Degree-day factor	mm/°C-day	0	10
	<i>SFCF</i>	Snowfall correction factor	—	0.5	1.5
	<i>CFR</i>	Refreezing coefficient	—	0	1
	<i>CWH</i>	Water holding capacity	—	0	1
<b>Soil moisture</b>	<i>FC</i>	Maximum soil moisture storage	mm	50	500
	<i>LP</i>	Soil moisture value above which AET=PET	mm	0	1
	<i>BETA</i>	Determines the relative contribution from rain / snowmelt to runoff	—	0.1	6
<b>Response</b>	<i>PERC</i>	Maximum rate of recharge between upper and lower groundwater reservoirs	mm/day	0	15
	<i>UZL</i>	Threshold for $Q_0$ flow	mm	0	100
	<i>K0</i>	1st recession coefficient	day <sup>-1</sup>	0.1	0.99
	<i>K1</i>	2nd recession coefficient	day <sup>-1</sup>	0.01	0.3
	<i>K2</i>	3rd recession coefficient	day <sup>-1</sup>	0.001	0.1
<b>Flood routing</b>	<i>MAXBAS</i>	Triangular weighting function length in routing	day	1	7

#### 4. RESULTS

Simulated streamflow was evaluated against observed streamflow using the Nash-Sutcliffe Efficiency, together with six other indicators described in Table 2, along with their values computed for the calibration and validation periods.

The HBV model managed to reproduce well the observed streamflow while keeping the parameters values physically meaningful (Fig. 3). Some simulated flood events had underestimated peak flows, while others were overestimated. Overall, the streamflow was underestimated (positive *PBIAS*) for both calibration and validation.

Table 2

Selected indices for performance assessment and their values for the calibration and validation

N° Index	Formula (Value range and Ideal value)	Calibra- tion	Valida- tion
1 <b>NSE</b> (Nash-Sutcliffe Efficiency)	$NSE = 1 - \frac{\sum_{i=1}^N (Q_{obs,i} - Q_{sim,i})^2}{\sum_{i=1}^N (Q_{obs,i} - \overline{Q_{obs}})^2}$ (Range: $-\infty \dots 1$ . Ideal value: <b>1</b> )	0.805	0.751
2 <b>MKGE</b> (Modified Kling-Gupta Efficiency)	where: $KGE = 1 - \sqrt{(r - 1)^2 + (\beta - 1)^2 + (\gamma - 1)^2}$ $r = \frac{\sum_{i=1}^N [(Q_{obs,i} - \overline{Q_{obs}})(Q_{sim,i} - \overline{Q_{sim}})]}{\sqrt{\sum_{i=1}^N (Q_{obs,i} - \overline{Q_{obs}})^2 \sum_{i=1}^N (Q_{sim,i} - \overline{Q_{sim}})^2}}; \beta = \frac{\overline{Q_{sim}}}{\overline{Q_{obs}}}; \gamma = \frac{\sigma_{sim}/\overline{Q_{sim}}}{\sigma_{obs}/\overline{Q_{obs}}}$ (Range: $-\infty \dots 1$ . Ideal value: <b>1</b> )	0.867	0.760
3 <b>PBIAS</b> (Percent Bias)	$PBIAS = 100 \frac{\sum_{i=1}^N (Q_{obs,i} - Q_{sim,i})}{\sum_{i=1}^N (Q_{obs,i})}$ (Range: $-100 \dots \infty$ . Ideal value: <b>0</b> )	8.198	12.305
4 <b>R<sup>2</sup></b> (Coefficient of Determination)	$R^2 = \left\{ \frac{\sum_{i=1}^N [(Q_{obs,i} - \overline{Q_{obs}})(Q_{sim,i} - \overline{Q_{sim}})]}{\sqrt{\sum_{i=1}^N (Q_{obs,i} - \overline{Q_{obs}})^2 \sum_{i=1}^N (Q_{sim,i} - \overline{Q_{sim}})^2}} \right\}^2$ (Range: $0 \dots 1$ . Ideal value: <b>1</b> )	0.814	0.763
5 <b>EV</b> (Explained Variance)	$EV = 1 - \frac{\sum_{i=1}^N [(Q_{sim,i} - Q_{obs,i}) - \frac{1}{N} \sum_{i=1}^N (Q_{sim,i} - Q_{obs,i})]^2}{\sum_{i=1}^N (Q_{obs,i} - \overline{Q_{obs}})^2}$ (Range: $-\infty \dots 1$ . Ideal value: <b>1</b> )	0.811	0.761
6 <b>MAE</b> (Mean Absolute Error)	$MAE = \frac{1}{N} \sum_{i=1}^N  Q_{obs,i} - Q_{sim,i} $ (Range: $0 \dots \infty$ . Ideal value: <b>0</b> )	0.439	0.435
7 <b>RMSE</b> (Root Mean Square Error)	$RMSE = \sqrt{\frac{1}{N} \sum_{i=1}^N (Q_{obs,i} - Q_{sim,i})^2}$ (Range: $0 \dots \infty$ . Ideal value: <b>0</b> )	0.553	0.604

The *Nash-Sutcliffe Efficiency* for the calibration period was 0.805, and for the validation one, 0.751, which represent good values, especially considering the large size of the river basin and its elevation range of ~2 km. The peak times of the floods were generally well reproduced.

The *Modified Kling-Gupta Efficiency* had slightly better scores for both calibration and validation, indicating that the HBV model was consistent in terms of peak timing, variability, and accuracy. If only the simulated streamflow is of interest, HBV has an advantage in terms of preprocessing and speed over spatially-distributed models, which provided similar results [15].

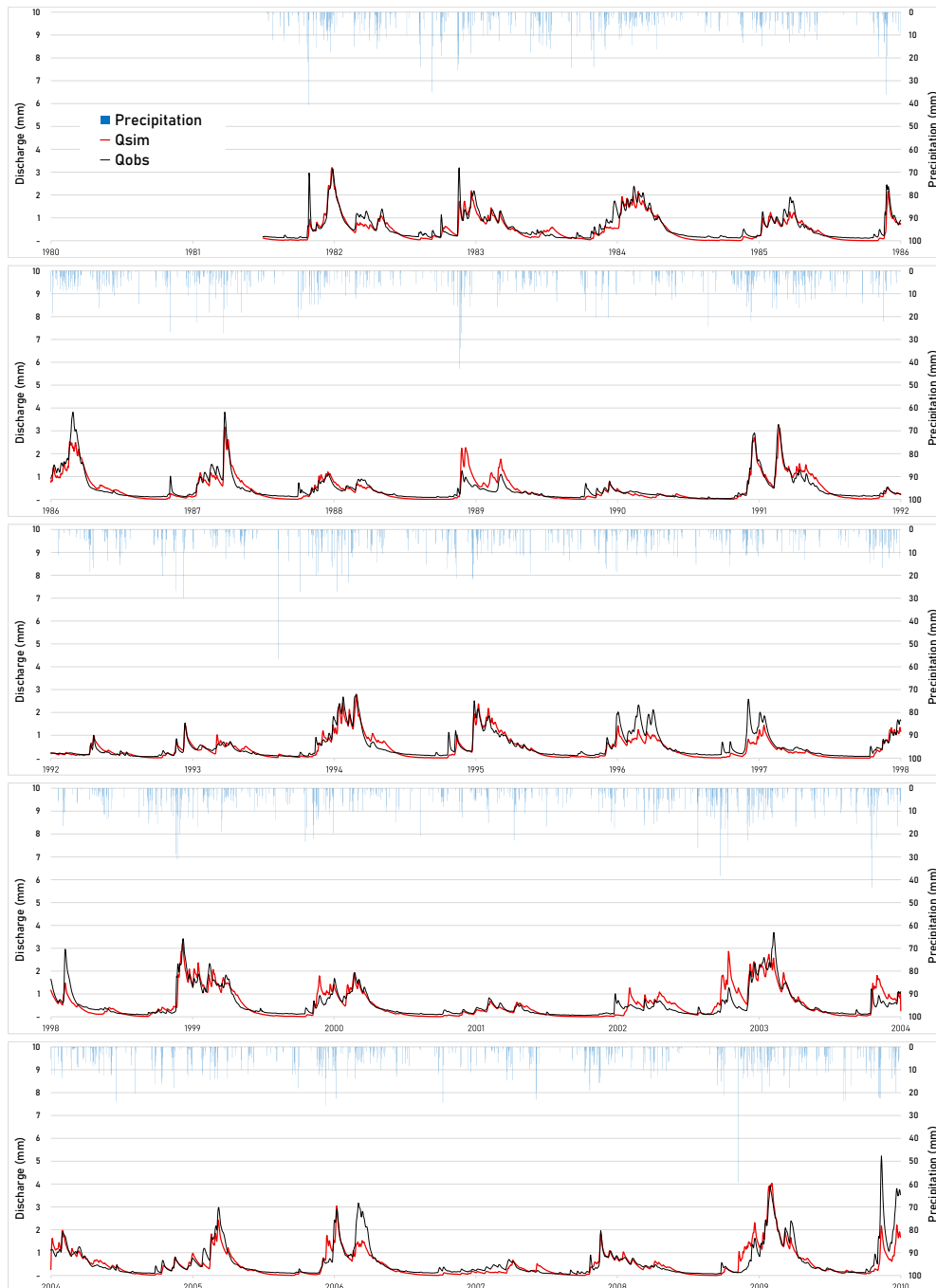


Fig. 3 – Simulated vs observed daily discharge over the calibration (1981–2003) and validation (2004–2009) periods.

Ewen et al. [16] classified the errors in physically-based rainfall-runoff models into three groups: *model structure errors* (related to the equations of the model); *parameter errors* (due to the parameter values used in the equations); and *run time errors* – associated with rainfall and other forcing data. While all the aforementioned errors affect the difference between simulated and observed runoff, their individual contributions cannot usually be isolated, as there is always a lack of knowledge about the catchment and its hydrological responses [16]. Also, changes in atmospheric circulation [17-19], air temperature [20,22], precipitation type [23,24] or land cover [25,26] could affect the streamflow regime over few decades. Last but not least, the low number of weather stations involved in the precipitation gridding might be another reason for the differences between the simulated and the observed discharge. While rain gauges provide accurate precipitation measurements at local scale, they are unable to properly represent the rainfall spatial distribution in sparsely gauged regions [27], in particular in mountainous river basins.

## 5. CONCLUSIONS

We presented the application of a conceptual rainfall-runoff model on a large river basin in northwestern Greece. The main conclusions are as follows:

- (1) the model provided satisfactory results, despite the sparse station data used in the gridding over the region, which probably underestimated the precipitation amount.
- (2) The HBV model was easy to setup and the visual interface looks ergonomic.
- (3) The model runs fast, allowing for an accurate automatic calibration.
- (4) The GAP optimization performed better than Monte Carlo (time-wise), providing a better set of parameters.

**Acknowledgements.** This study was done within the project “Intelligent asset Management Platform for Hydropower operation & maintenance” (iAMP-Hydro) funded by the European Union’s Horizon Europe research and innovation programme under grant agreement N° 101122167.

## REFERENCES

1. E.Z. Pebesma, P. Switzer, and K. Loague, *Error analysis for the evaluation of model performance: rainfall–runoff event summary variables*. Hydrol. Process. **21**, 3009–3024 (2007).
2. M.V. Birsan, *Application of a distributed physically-based hydrological model on the upper river basin of Someşul Mare (northern Romania)*. Rom. Rep. Phys., **65**(4), 1469–1478 (2013).
3. S. Bergström, *The HBV Model: Its Structure and Applications*, Swedish Meteorological and Hydrological Institute (SMHI), Hydrology, Norrköping, 35 pp. (1992).
4. M. Mimikou and F. Fotopoulos, *Regional effects of climate change on hydrology and water resources in Aliakmon River basin*. In: Regional Hydrological Impacts of Climatic Change—Impact Assessment and Decision Making (Proceedings of symposium S6 held during the Seventh IAHS Scientific Assembly, Foz do Iguaçu, Brazil, April 2005). IAHS Publication N° 295 (2005).
5. R.C. Cornes, et al, *An ensemble version of the E-OBS temperature and precipitation data sets*. J. Geophys. Res. Atmos. **123** (17), 9391–9409 (2018). [10.1029/2017JD028200](https://doi.org/10.1029/2017JD028200)

6. D.N. Karger, et al., *Climatologies at high resolution for the Earth land surface areas*. Sci. Data. 4, 170122 (2017). <https://doi.org/10.1038/sdata.2017.122>
7. D.N. Karger, et al., *Data from: Climatologies at high resolution for the Earth's land surface areas*. EnviDat (2018). <https://doi.org/10.16904/envidat.228.v2.1>
8. P. Brun, et al., *Global climate-related predictors at kilometre resolution for the past and future*. Earth Syst. Sci. Data 14, 5573–5603 (2022). <https://doi.org/10.5194/essd-14-5573-2022>
9. P. Brun, et al., *CHELSEA-BIOCLIM+ A novel set of global climate-related predictors at kilometre-resolution*. EnviDat. (2022) <https://www.doi.org/10.16904/envidat.332>
10. S. Bergström, *The HBV model*. Chapter 13 in: V.P. Singh (Ed.) Computer Models of Watershed Hydrology, Water Resources Publications, Highlands Ranch, Colorado, USA, 443–476, (1995).
11. J. Seibert J and S. Bergström, *A retrospective on hydrological catchment modelling based on half a century with the HBV model*. Hydrol. Earth Syst. Sci., **26**, 1371–1388 (2022).
12. J. Seibert, *Multi-criteria calibration of a conceptual runoff model using a genetic algorithm*. Hydrol. Earth Syst. Sci. **4**, 215–224 (2000). <https://doi.org/10.5194/hess-4-215-2000>
13. J. Seibert and M.J.P. Vis, *Teaching hydrological modeling with a user-friendly catchment-runoff-model software package*. Hydrol. Earth Syst. Sci. **16**, 3315–3325.
14. M. Karamouz, E. Goharian, and S. Nazif, *Reliability Assessment of Water Supply Systems under Uncertain Future Extreme Climate Conditions*. Earth Interact. **17**(20), 1–27 (2013).
15. D. Frysalı, Z. Mallios, and N. Theodossiou, *Hydrologic modeling of the Aliakmon River in Greece using HEC–HMS and open data*. Euro-Mediterr. J. Environ. Integr. **8**, 539–555 (2023).
16. J. Ewen, G. O'Donnell, A. Burton, and E. O'Connell, *Errors and uncertainty in physically-based rainfall-runoff modelling of catchment change effects*. J. Hydrol. **330**(3–4), 641–650 (2006).
17. M.V. Birsan, I.A. Nita, V.A. Amihăesci, *Influence of large-scale atmospheric circulation on Romanian snowpack duration*. Rom. Rep. Phys. **76**, 708 (2024). <https://doi.org/10.59277/RomRepPhys.2024.76.708>
18. I.A. Nita, L. Apostol, C.V. Patriche, L. Sfică, R. Bojariu, M.V. Birsan, *Frequency of Atmospheric Circulation Types over Romania According to Jenkinson–Collison Method Based on Two Long-Term Reanalysis Datasets*. Rom. J. Phys. **67**, 812 (2022)
19. M.V. Birsan, *Trends in monthly natural streamflow in Romania and linkages to atmospheric circulation in the North Atlantic*. Water Resour. Manage. **29**, 3305–3313 (2015). <https://doi.org/10.1007/s11269-015-0999-6>
20. I.A. Nita, et al., *Changes in the global mean air temperature over land since 1980*. Atmos. Res. **279**, 106392 (2022). <https://doi.org/10.1016/j.atmosres.2022.106392>
21. C. Necula, et al., *Maximum winter temperature over Romania in connection to atmospheric circulation*, Theor. Appl. Climatol. **155**, 3861–3870 (2024). <https://doi.org/10.1007/s00704-024-04854-5>
22. L. Boboc, et al., *Trends and variability of heat waves in Europe and the association with large-scale circulation patterns*. Weather and Climate Extremes **49**, 100794 (2025).
23. A. Manea, M.V. Birsan, G. Tudorache, and F. Cărbunaru, *Changes in the type of precipitation and associated cloud types in Eastern Romania (1961–2008)*. Atmos. Res. **169**, 357–365 (2016). <https://doi.org/10.1016/j.atmosres.2015.10.020>
24. A. Busuioc, et al., *Changes in the large-scale thermodynamic instability and connection with rain shower frequency over Romania. Verification of the Clausius–Clapeyron scaling*. Int. J. Climatol. **36**, 2015–2034 (2016). <https://doi.org/10.1002/joc.4477>
25. G. Mihai, et al., *Impact of Climate Change and Adaptive Genetic Potential of Norway Spruce at the South–eastern Range of Species Distribution*. Agr. Forest Meteorol. **291**, 108040 (2020). <https://doi.org/10.1016/j.agrformet.2020.108040>
26. G. Mihai, et al., *Intraspecific Growth Response to Drought of Abies alba in the Southeastern Carpathians*. Forests **12**(4), 387 (2021). <https://doi.org/10.3390/f12040387>
27. C.M. Stephens, H.T. Pham, L.A. Marshall, and F.M. Johnson, *Which rainfall errors can hydrologic models handle? Implications for using satellite-derived products in sparsely gauged catchments*. Water Resour. Res. **58**, e2020WR029331 (2022).